Inorganic Chemistry

Article

pubs.acs.org/IC

Shape Modulation of Octanuclear Cu(I) or Ag(I) Dichalcogeno Template Clusters with Respect to the Nature of their Encapsulated Anions: A Combined Theoretical and Experimental Investigation

Camille Latouche,[†] Samia Kahlal,[†] Eric Furet,[†] Ping-Kuei Liao,[‡] Yan-Ru Lin,[‡] Ching-Shiang Fang,[‡] Jérôme Cuny,[§,∥] C. W. Liu,*[,‡] and Jean-Yves Saillard*[,†]

[†]Institut des Sciences Chimiques de Rennes, UMR 6226 CNRS, Université de Rennes 1, Ecole Nationale Supérieure de Chimie de Rennes, Avenue du Général Leclerc, 35042 Rennes, France

[‡]Department of Chemistry, National Dong Hwa University, Hualien, Taiwan 97401, Republic of China

[§]Department of Chemistry and Applied Biosciences, ETH Zurich, Zurich, Switzerland

[∥]Facoltà di Informatica, Istituto di Scienze Computazionali, Università della Svizzera Italiana, Via G. Buffi 13, 6900 Lugano, Switzerland

Supporting Information

ABSTRACT: M_8L_6 clusters (M = Cu(I), Ag(I); L = dichalcogeno ligand) are known for their ability to encapsulate various kinds of saturated atomic anions. Calculations on the models $[M_8(E_2PH_2)_6]^{2+}$ (M = Cu(I), Ag(I); E = S, Se) and the ionic or neutral $[M_8(X)(E_2PH_2)_6]^q$ (X = H, F, Cl, Br, O, S, Se, N, P, C) indicate that the cubic M_8L_6 cage adapts its shape for maximizing the host−guest bonding interaction. The interplay between size, covalent and ionic bonding favors either a cubic, tetracapped tetrahedral, or bicapped octahedral structure of the metal framework. Whereas the large third- and fourth-row main group anions maintain the cubic shape, a distortion toward a tetracapped tetrahedral arrangement of the metals occurs in the case of hydride, fluoride, and oxide. The distortion is strong in the case of hydride, weak in the case of fluoride, and intermediate in the case of oxide. Density functional theory (DFT) calculations predict a bicapped octahedral architecture in the case of nitride and carbide. These computational results are supported by X-ray structures, including those of new fluorine- and oxygen-containing compounds. It is suggested that other oxygen-containing as well as so far unknown nitride-containing clusters should be feasible. For the first time, the dynamical behavior of the encapsulated hydride has been investigated by metadynamics simulations. Our results clearly demonstrate that the interconversion mechanism between two identical tetracapped tetrahedral configurations occurs through a succession of M-H bonds breaking and forming which present very low activation energies and which involve a rather large number of intermediate structures. This mechanism is full in accordance with ^{109}Ag and ^{1}H state NMR measurements.

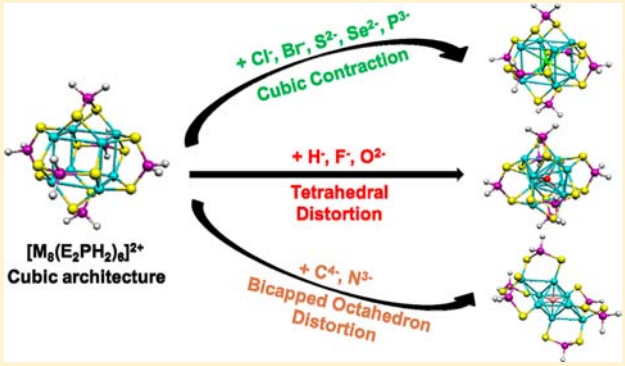

1. INTRODUCTION

Cu(I) and Ag(I) are known to form polynuclear clusters and polymers with various types of bridging chalcogen donor ligands.[1] The stability of the Cu_n or Ag_n framework is mainly ensured by the chelating effect of the ligands, although weak d^{10}-d^{10} bonding interactions between the closed-shell metal centers is also present. As a result, the polynuclear metallic cage is rather flexible and can easily adjust its size and shape for encapsulating various types of atomic anions which bind to their hosting cage through both ionic and covalent interactions.[2−10] From this point of view, the use of the dithio- and diseleno-phosphate monoanionic ligands ($(E_2P(OR)_2)^-$, E = S, Se) allows the formation of cationic cluster cages which are particularly well suited for anion encapsulation. For example, octanuclear dithio- and diseleno-phosphate cubic clusters of the type $[M_8(E_2P(OR)_2)_6]^{2+}$ (M = Cu, Ag; E = S, Se) can easily entrap a halide, a chalcogenide, or a hydride ion.[7,8] Whereas in the general case the incorporation of an anion inside the cubic host cage modifies its size, but not its cubic shape, in the case of hydride, the octanuclear cage affords, upon encapsulation, a distortion from cubic to tetracapped tetrahedral shape[7−9] (Scheme 1a and Scheme 2) in such a way that the hydride is tetracoordinated, that is, $[M_4(\mu_4\text{-H})(\mu_3\text{-M})_4(E_2P(OR)_2)_6]^+$.[7,8] Previous calculations have also shown that the small fluorine anion also induces such tetracapped tetrahedral distortion,[7a] but in that particular case the predicted distortion is small and therefore difficult to be experimentally verified, being (if any)

Received: April 18, 2013
Published: June 10, 2013

   dx.doi.org/10.1021/ic400959a | Inorg. Chem. 2013, 52, 7752−7765

Scheme 1. M_8 Cube Prepared for Various Distortions: (a) Symmetry of the Bare M_8 cube; (b) Symmetry of the Whole $[M_8(E_2P(OR_2)_6)]^{2+}$ Cluster

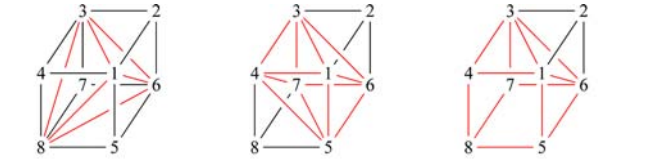

buried among other distortions arising from unsymmetrical steric and crystal packing forces.

Since such clusters are susceptible to entrap various kinds of anions which could lead to different shape modifications of the host cage, we have undertaken a comprehensive theoretical investigation of an homogeneous series of octanuclear Cu(I) and Ag(I) dithio- and diseleno-phosphine clusters encapsulating various atomic anions from Group 14 to Group 17, as well as hydride for the sake of comparison. The cluster shape, stability, and the host-cage bonding are analyzed in terms of anion size, charge effect, and covalency. The potential dynamic behavior of some of them is also investigated. The following monometallic model clusters have been computed: $[M_8(X)(E_2PH_2)_6]^q$ (M = Cu, Ag ; X = □ (vacancy), q = +2; X = H, F, Cl, Br, q = +1; X = O, S, Se, q = 0; X = N, P, q = −1; X = C, q = −2; E = S, Se), as well as the homologous bimetallic species $[Cu_4Ag_4(X)(E_2PH_2)_6]^q$ (X = □, H, F, Cl, Br, O, S, Se; E = S, Se).

To compare our theoretical predictions to experimental facts, we have also carried out the structural analysis of some of the computed compounds, namely, fluoride- and oxide-centered species, the latter being a bimetallic Cu_4Ag_4 species.

2. COMPUTATIONAL DETAILS

2.1. Static Calculations. Density functional theory (DFT) calculations were carried out using the Gaussian 03 package,[11] employing the BP86 functional,[12] and using the general triple-ξ polarized basis set, namely, the Def2-TZVP set from EMSL Basis Set Exchange Library.[13] Such functional and basis sets were chosen as the result of systematic investigation of geometry of Cu(I) and Ag(I) model complexes carried out in our laboratory and comparison with experimental structures and post-HF calculations. We have shown that, although they are not designed for accounting properly for d^{10}-d^{10} interactions, they provide among the best results for a reasonable computational demand. In particular, we found that the use of functionals containing long-range dispersion corrections did not improve significantly the structural results and provided similar trends in the binding energies. All stationary points were fully characterized as true minima via analytical frequency calculations. Geometries obtained from DFT calculations were used to perform natural orbital analysis with the NBO 5.0 program.[14]

2.2. Molecular Dynamics Calculations. The molecular dynamics (MD) simulations have been performed within the Car−Parrinello formalism using the CPMD code,[15] using the BP86 functional. The core valence interactions were described using fully nonlocal norm-conserving pseudopotentials as proposed by Troullier and Martins[16] in combination with an 80 Ry plane-wave energy cutoff and a Γ point sampling of the first Brillouin zone. To reproduce the molecular character of the simulated species, a 16 Å cubic supercell that allows minimizing the interactions between the periodic images of our system was used. The fictitious electron mass was set to 320 au, the time step to 0.075 fs, and the temperature was controlled using a colored-noised Langevin thermostat.[17] Metadynamics (MetaD) simulations were performed using the CPMD code in combination with the PLUMED package v. 1.2.[18] The well-tempered formulation of MetaD was used,[19] with an initial hill height of 0.000475 hartree, a deposit stride of 18.3 fs, a Gaussian width of 0.19. The collective variables (CVs) were sampled at a fictitious temperature of 3000 K. Finally, the coordination number CVs were defined using the following continuous switching function:

$$CV = \sum_j \frac{\left(1 - \frac{r_{ij} - d_0}{r_0}\right)^n}{\left(1 - \frac{r_{ij} - d_0}{r_0}\right)^m}$$

where i stands for the hydride, j for the Cu atoms, r_{ij} is the corresponding distance expressed in Bohr, d_0 and r_0 are distances and n and m are integers. We have chosen the following values d_0 = 3.21 Bohr, r_0 = 0.59 Bohr, n = 6, and m = 12 so as to get a proper discrimination between bonded and nonbonded atoms. The coordination number of the hydride with one Cu is thus equal to 1 when $r_{ij} < d_0$ and to CV when $r_{ij} > d_0$.

3. EXPERIMENTAL SECTION

Procedures for Single Crystal X-ray Crystallography. The synthesis and characterizations of compounds **1**−**4** are described in the Supporting Information. Single crystals were grown by diffusion of hexane into an acetone solution of **1** and **2**, THF solution of **3** at −20

Scheme 2. Tetrahedral Distortion Afforded by the Cage $[M_8(E_2P(OR)_2)_6]^{2+}$ (M = Cu, Ag; E = S, Se) upon Encapsulation of H^-[a]

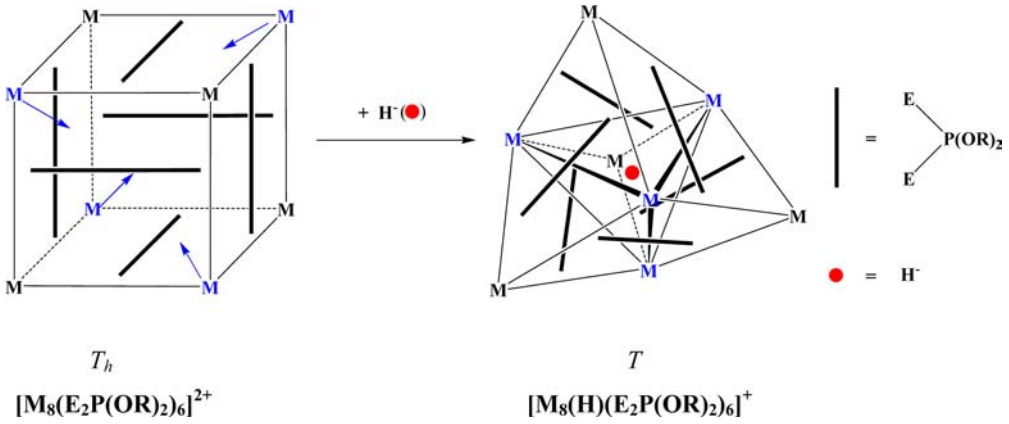

[a]The 12 edges of the metal cube are bridged by the 6 (μ_2, μ_2) di-chalcogeno ligands.

dx.doi.org/10.1021/ic400959a | Inorg. Chem. 2013, 52, 7752−7765

Table 1. Selected Crystallographic Data for $[Cu_8(F)(S_2P(OR)_2)_6](PF_6)$ (R = ^{i}Pr, 1; R = Et, 2), $[Ag_8(F)(S_2P(O^nPr)_2)_6](PF_6)$ (3) and $Cu_4Ag_4(O)(Se_2P(OEt)_2)_6$ (4)

	1	2	3	4
formula	$C_{36}H_{84}Cu_8F_7O_{12}P_7S_{12}$	$C_{24}H_{60}Cu_8F_7O_{12}P_7S_{12}$	$C_{36}H_{84}Ag_8F_7O_{12}P_7S_{12}$	$C_{24}H_{60}Ag_4Cu_4O_{13}P_6S_{12}$
Fw	1951.86	1783.55	2306.50	1812.90
space group	$C2/c$	$R\bar{3}c$	$R\bar{3}$	$R\bar{3}$
a, Å	23.9882(11)	17.4297(9)	21.7439(11)	21.164(2)
b, Å	12.8099(6)	17.4297(9)	21.7439(11)	21.164(2)
c, Å	24.5399(11)	72.762(4)	13.8873(7)	11.719(2)
α, deg	90	90	90	90
β, deg	90.8310(10)	90	90	90
γ, deg	90	120	120	120
V, Å^3	7540.0(6)	18880.2(18)	5686.2(5)	4546.1(9)
Z	4	12	3	3
ρ_{cald}, g cm^{-3}	1.719	1.882	2.021	1.987
μ, mm^{-1}	2.754	3.290	2.562	3.256
T, K	296(2)	296(2)	296(2)	296(2)
reflection collected	32678	17487	15784	13355
independent reflections	6636 [R_{int} = 0.0369]	3710 [R_{int} = 0.0494]	3136 [R_{int} = 0.0279]	2538 [R_{int} = 0.0364]
$R1$,[a] wR_2[b] [$I > 2\sigma(I)$]	0.0474, 0.1269	0.0588, 0.1714	0.0412, 0.1104	0.0639, 0.1918
$R1$,[a] $wR2$[b] (all data)	0.0625, 0.1411	0.0812, 0.2036	0.0585, 0.1271	0.0985, 0.2266
GOF	1.044	1.068	1.029	1.050
large diff peak and hole, e/Å^3	1.211 and −0.721	1.812 and −0.698	0.938 and −0.532	0.714 and −1.007

[a] $R1 = \sum||F_o| - |F_c||/\sum|F_o|$. [b] $wR_2 = \{\sum[w(F_o^2 - F_c^2)^2]/\sum[w(F_o^2)^2]\}^{1/2}$.

°C, and $CHCl_3$ solution of **4**. Crystals **1**−**4** were mounted on the tip of glass fibers with epoxy resin.

X-ray diffraction analyses of the crystals were performed on a Bruker APEX II CCD diffractometer using graphite monochromated Mo Kα radiation (λ = 0.71073 Å). Data reduction was performed with SAINT,[20] which corrects for Lorentz and polarization effects. A multiscan absorption correction based on SADABS was applied.[21] Structures were solved by the use of direct methods, and the refinements were performed by the least-squares methods on F^2 with the SHELXL-97 package,[22] incorporated in SHELXTL/PC V5.10.[23] All Cu and Ag atoms in **4** were disordered over two positions, each being 50% probability. Restraints to the alkyl side chains and PF_6^- anion were applied in some cases. H atoms on the alkyl side chains were added at idealized positions. Relevant crystallographic data for compounds **1**−**4** are given in Table 1.

4. GEOMETRICAL ANALYSIS OF THE COMPUTED STRUCTURES

4.1. Copper Clusters. We first discuss the copper clusters made of dithio ligands (E = S). As illustrated in Scheme 2, each square face of the cube is bridged by a dichalcogeno ligand which adopts a tetrametallic tetraconnective (μ_2, μ_2) coordination pattern. It follows that the regular cubic architecture is of T_h (not O_h) symmetry, and the tetracapped tetrahedral one is of T (not T_d) symmetry. All the models were first computed under both the T_h and T symmetry constrains. It turned out that, as in the cases of the empty cage (X = □), the presence of an encapsulated anion from the third or fourth period resulted in a cubic global energy minimum of T_h symmetry, that is, optimizations in T symmetry ended up with the same geometries as those obtained assuming T_h symmetry constraint (Table 2). As an example, the optimized structure of $[Cu_8(Cl)(S_2PH_2)_6]^+$ is shown in Figure 1. Such a symmetrical architecture has been previously described as displaying a chalcogen icosahedron circumscribing an M_8 cube or a dodecahedron made of the chalcogen and metal atoms all together.[24] When the encapsulated anion is a hydride or an anion from the second period, the optimized T_h structure was found to be associated with several imaginary frequency calculations (Table 2), indicating that this cubic structure is not a minimum on the potential energy hypersurface. In the case of X = H and F, the tetracapped tetrahedral structure of T symmetry (see Figure 1) was found to be the global minimum. These results are in agreement with our previous calculations on Cu(I) and Ag(I) diseleno clusters containing encapsulated hydrides and halogenides.[7a,8a] As mentioned above, in the case of X = H they are consistent with all the known X-ray structures.[7−10] One should also mention that, during this current investigation, two additional secondary minima were found for X = H. They are not reported in Table 2 and will be discussed in a next section.

The energy stabilization gained when going from the T_h structure to the T one is substantial in the case of X = H (0.42 eV) and very small in the case of X = F (0.01 eV). Consistently, the tetracapped tetrahedral distortion is larger in the case of H. The magnitude of this distortion can be evaluated by the following distortion index (DI):

$$DI(\%) = (\sqrt{2} + 1)[\sqrt{2} - (d_{13}/d_{12})] \times 100$$

where d_{12} and d_{13} are the M(1)−M(2) and M(1)−M(3) distances respectively (see left side of Scheme 1). In the case of a perfect T_h cubic structure, DI = 0%, whereas DI = 100% for the ideal case of a tetracapped tetrahedron in which all the Cu(tetrahedron)-Cu(tetrahedron) and Cu(cap)-Cu(tetrahedron) distances are equal ($d_{12} = d_{13}$), that is, for a regular stellated tetrahedron.[25] One should note that this latter ideal value is almost never reached in the known experimental tetracapped tetrahedral structures of hydride-containing dithio- and diseleno- octanuclear clusters for which average DI values vary between 55% and 102% (see Table 3), although the lowest ones are probably underestimated because of the presence of severe disorder in the crystal structure.

In the case of X = H, the computed DI is equal to 81%, indicating clearly a tetracapped tetrahedral shape with the hydride only bonded to four copper atoms (Cu−H = 1.77 Å).

dx.doi.org/10.1021/ic400959a | Inorg. Chem. 2013, 52, 7752−7765

Table 2. Relevant Computed Data Corresponding to the Optimized Geometries of $[Cu_8(X)(S_2PH_2)_6]^q$ (X = □ (vacancy), H, F, Cl, Br, O, S, Se, N, P, C)[a]

q	$[Cu_8(X)(S_2PH_2)_6]^q$	symm.	imag. freq. (cm^{-1})	ΔE (eV)[b]	Cu_1–Cu_2 (Å) Cu_1–Cu_3 (Å)	Cu_1–X (Å) Cu_2–X (Å)	DI (%)[c]
+2	X = □	T_h			3.21		0
					4.54		
+1	X = H	T		0.00	2.69	1.77	81
					2.90	2.69	
		T_h	356.i (t_u), 60.i (a_u), 36.i (t_g)	0.42	2.61	2.26	0
					3.69		
	X = F	T		0.00	2.98	2.44	19
					3.98	2.71	
		T_h	71.i (t_u), 32.i (a_u)	0.01	2.97	2.58	0
					4.21		
	X = C1	T_h		0.00	3.16	2.74	0
					4.47		
	X = Br	T_h		0.00	3.22	2.97	0
					4.55		
0	X = O	T		0.00	2.78	2.05	50
					3.36	2.68	
		T_h	65.i (a_u), 18.i (t_g)	0.18	2.70	2.34	0
					3.82		
	X = S	T_h		0.00	2.84	2.46	0
					4.02		
	X = Se	T_h		0.00	2.95	2.55	0
					4.17		
−1	X = N	S_6		0.00	6×2.67, 6×2.75, 6×2.92	6×1.92, 2×3.53	
		C_3		1.20	3×2.57, 3×2.58, 3×2.61, 3×2.66, 3×2.71	3×2.19, 3×2.00, 1×2.14, 1×3.35	
		T_h	60.i (a_u), 19.i (t_g)	1.49	2.56	2.21	0
					3.62		
	X = P	T_h		0.00	2.73	2.36	0
					3.85		
−2	X = C	S_6		0.00	6×2.76, 6×2.65, 6×2.80	6×1.91, 2×3.36	
		T_h	26.i (t_g), 24.i (t_u), 23.i (e_u)	3.05	2.49	2.16	0
					3.52		

[a]The metal atom numbering corresponds to that of Scheme 1 (left side) and refers to the values of the T_h and T structures only. [b]Relative energies between different geometries of the same compound. [c]Distortion index measuring the degree of tetrahedral distortion away from the ideal T_h cubic structure, as defined in the text.

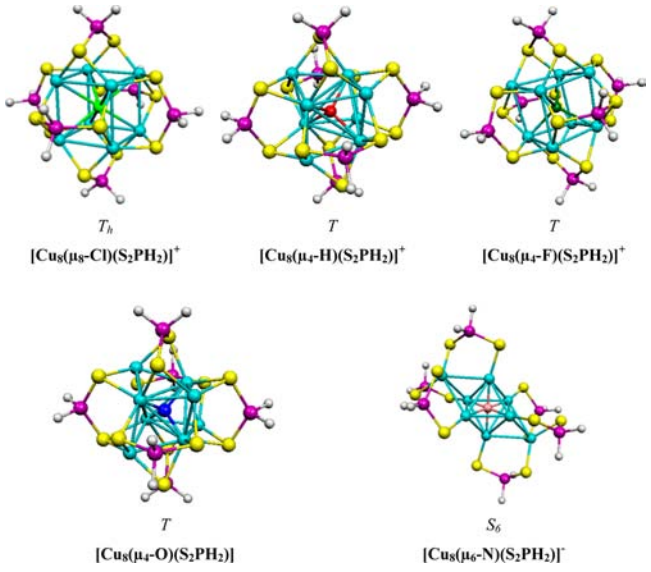

Figure 1. Selected optimized structures in their global energy minima.

On the other hand, DI = 19% when X = F, which means that fluorine is still somehow octacoordinated but with two different sets of four Cu–F distances, one short (2.44 Å) and one long (2.71 Å). Surprisingly, although the oxo anion is bigger than fluoride and therefore may be thought to favor octacoordination even more strongly, the T structure was found significantly more stable than the T_h one in this case, the T_h geometry being not an energy minimum. Consistently, with DI equal to 50%, the tetrahedral distortion is pronounced and the two sets of Cu–O distances (2.05 Å and 2.68 Å) indicate clearly tetracoordination (see Figure 1). When X = N, the T structure is also found more stable than the T_h one but with a smaller difference than the oxo anion case (0.10 eV). Moreover, imaginary frequencies are computed for both T and T_h structures. Following the atomic displacements associated with the imaginary frequencies of the T structure resulted in the finding of a global minimum of S_6 symmetry in which the nitrogen atom sits in the middle of a bicapped octahedron of copper atoms. The distortion of the regular cubic arrangement to the bicapped octahedral structure of the Cu_8 core is sketched in the middle of Scheme 1. The optimized structure is shown in Figure 1. One should note that this is the presence of the dithio chelating ligands which lowers the bicapped octahedral

dx.doi.org/10.1021/ic400959a | Inorg. Chem. 2013, 52, 7752–7765

Table 3. Approximate Experimental Values of the Distortion Index (DI)[a] Measuring the Degree of Tetrahedral Distortion in Hydride-Containing Dithio- and Diseleno- Octanuclear Clusters, Assuming an Averaged Ideal Structure of *T* Symmetry

compound	reference	M_1-M_2(Å)[b] M_1-M_3(Å)	DI (%)
$[Cu_8(H)(S_2P(O^iPr)_2)_6]^+$	7b	2.731 3.002	76
$[Cu_8(H)(S_2P(OEt)_2)_6]^+$ (molecule 1)	7b	2.749 2.977	80
$[Cu_8(H)(S_2P(OEt)_2)_6]^+$ (molecule 2)	7b	2.719 3.121	64
$[Cu_8(H)(Se_2P(O^iPr)_2)_6]^+$	7a	2.759 2.991	80
$[Cu_8(H)(Se_2P(OEt)_2)_6]^+$	7a	2.718 2.934	81
$[Ag_8(H)(S_2P(OEt)_2)_6]^+$	8b	3.159 3.133	102
$[Ag_8(H)(Se_2P(O^iPr)_2)_6]^+$	8a	3.034 3.163	90
$[Ag_8(H)(Se_2P(OEt)_2)_6]^+$	8a	3.108 3.129	98
$[Cu_8(H)(S_2CC(CN)_2)_6]^{5-}$ (molecule 1)	9a	2.600 3.031	60
$[Cu_8(H)(S_2CC(CN)_2)_6]^{5-}$ (molecule 2)	9a	2.592 3.074	55
$[Ag(H)(S_2CC(CN)_2)_6]^{5-}$ (molecule 1)	9a	2.894 3.290	67
$[Ag_8(H)(S_2CC(CN)_2)_6]^{5-}$ (molecule 2)	9a	2.897 3.210	74
$[Cu_8(H)(S_2CN^nPr_2)_6]^+$	9b	2.613 2.926	71
$[Cu_8(H)(S_2CNEt_2)_6]^+$	9b	2.586 2.929	68
$[Cu_8(H)(Se_2P(CH_2CH_2Ph)_2)_6]^+$	9c	2.736 2.912	84

[a]See text for the definition of DI. [b]Averaged experimental data (from X-ray structures).

symmetry from D_{3d} to S_6 and that the actual octahedral core is slightly elongated. Therefore, in this S_6 energy minimum, the nitride ion sits in the middle of an octahedral site and the six metal atoms constituting this octahedron are now bonded to only one sulfur atom. Interestingly, running the geometry optimization in the lower C_3 symmetry ended up with another energy minimum, of substantially higher energy (ΔE = 1.20 eV), in which the nitride is no more sitting in the middle of the octahedral site, but is shifted along the C_3 axis toward one of the metals capping the octahedron (Cu(8) on the right side of Scheme 1), whereas the three edges of the Cu(4)−Cu(5)−Cu(7) octahedron open up, as illustrated in Scheme 1 (right side). The encapsulated nitride is now bonded to the seven copper atoms constituting the red polyhedron shown on the right side of Scheme 1. When X = C, the energy minimum was also found to be a centered bicapped octahedron of S_6 symmetry but no other skeletal isomer could be found in this case.

The unexpected finding of S_6 and/or C_3 energy minima for X = C and N urged us to check the possibility of their existence for the other encapsulated elements. Only in the case of X = O, was a minimum of S_6 symmetry, that is, with O lying in the center of a Cu_8 bicapped octahedron, found. However, this skeletal isomer was found to lie far above the *T* minimum (1.92 eV) and will not be discussed further in this paper.

Rather similar results were obtained for the copper clusters containing diseleno ligands (Table 4 and Supporting Information, Table S1), however with some quantitative differences. The optimized $[Cu_8(□)(Se_2PH_2)_6]^{2+}$ empty cage is of somewhat larger size than its dithio analogue (Cu−Cu = 3.38 Å). Encapsulated anions from the third or fourth period resulted in T_h geometries with Cu−Cu distances slightly longer than in the dithio derivatives, except for X = P. In the case of encapsulated anions from the second period, as well as for hydride, the same distortion away from T_h was found, but it is energetically slightly more favored, and consistently structurally more pronounced, in the diseleno series (larger DI values). For X = N, in contrast to dithio ligands, the heptacoordinated C_3 minimum lies very close in energy to the hexacoordinated S_6 global minimum (ΔE = 0.01 eV). This is likely due to a larger cage flexibility of the diseleno cage, as compared to the dithio one.

4.2. Silver Clusters. With Ag−Ag distances equal to 3.59 Å (E = S) and 3.62 Å (E = Se), the $[Ag_8(□)(E_2PH_2)_6]^{2+}$ empty cages offer larger space (and likely larger flexibility) to potential encapsulated anions than their copper analogues (Cu−Cu = 3.38 Å). Nevertheless, the optimized structures of the silver models (Supporting Information, Tables S2 and S3) are qualitatively similar to those of their copper counterpart, that is, T_h cubic structures for encapsulated third and fourth-row anions, tetrahedrally distorted *T* structures for X = H, F, and O,

dx.doi.org/10.1021/ic400959a | Inorg. Chem. 2013, 52, 7752−7765

Table 4. Relevant Energetic and Structural Data Corresponding to the Energy Minima of $[M_8(X)(E_2PH_2)_6]^q$ (M = Cu, Ag; E = S, Se; X = □ (vacancy), H, F, Cl, Br, O, S, Se, N, P, C)

			M–X (Å)				ΔE (eV)[a]				DI (%)[b]			
q	X	symm	Cu/S	Cu/Se	Ag/S	Ag/Se	Cu/S	Cu/Se	Ag/S	Ag/Se	Cu/S	Cu/Se	Ag/S	Ag/Se
+2	□	T_h	2.78	2.93	3.06	3.14					0	0	0	0
−1	H	T	1.77	1.76	2.00	1.98	0.42	0.54	0.59	0.66	81	86	88	92
			2.69	2.73	3.15	3.18								
	F	T	2.44	2.37	2.55	2.53	0.01	0.04	0.03	0.04	19	33	30	36
			2.71	2.84	3.01	3.07								
	Cl	T_h	2.74	2.79	2.96	2.98					0	0	0	0
	Br	T_h	2.79	2.84	2.98	3.02					0	0	0	0
0	O	T	2.05	2.02	2.36	2.33	0.18	0.33	0.04	0.09	50	59	36	44
			2.68	2.75	2.86	2.93								
	S	T_h	2.46	2.46	2.74	2.76					0	0	0	0
	Se	T_h	2.55	2.56	2.81	2.83					0	0	0	0
−1	N	S_6	6×1.92	6×1.97	6×2.20	6×2.21	1.49	0.45	1.48	0.95				
			2×3.53	2×3.24	2×3.78	2×3.74								
		C_3	3×2.19	3×2.17	3×2.30	3×2.49								
			3×2.00	3×2.01	3×2.44	3×2.31	1.20	0.01	0.98	0.39				
			2.14	2.13	2.47	2.41								
			3.35	3.39	3.80	3.78								
	P	T_h	2.36	2.36	2.64	2.65					0	0	0	0
−2	C	S_6	6×1.91	6×1.92	6×2.18	6×2.19	3.05	1.83	3.21	2.70				
			2×3.36	2×3.31	2×3.68	2×3.69								

[a] ΔE = relative energy of the same cluster obtained when optimized under T_h symmetry constraint (see Table 2). [b] Distortion index measuring the degree of tetrahedral distortion away from the ideal T_h cubic structure, as defined in the text.

and S_6 or C_3 structures for nitride and carbide. However, the stabilization energy afforded upon tetrahedral distortion for the oxo species is smaller than in their copper relatives and consequently the DI value is also lower (Table 4). On the other hand, the tetrahedral distortion is energetically more favored and more pronounced in the case of hydride and fluoride when M = Ag. In the case of X = N and C, the energy minimum was also found to adopt the bicapped octahedral arrangement of S_6 symmetry, with a secondary minimum of C_3 symmetry for the nitride. When M = Cu, this secondary minimum in which N is heptacoordinated lies closer in energy to the S_6 global minimum in the case of diseleno ligands.

4.3. Mixed Cu_4/Ag_4 Clusters. Starting from a $[Cu_8(H)(Se_2P(OR)_2)_6]^+$ cluster in its stable tetracapped tetrahedral structure of ideal T symmetry and replacing formally four Cu atoms by four Ag atoms in the most symmetrical way results in two possible skeletal arrangements, still of T symmetry: a copper tetrahedron tetracapped by four silver atoms, that is, $[Cu_4(\mu_4\text{-}H)(\mu_3\text{-}Ag)_4(Se_2P(OR)_2)_6]^+$, or a silver tetrahedron tetracapped by four copper atoms, that is, $[Ag_4(\mu_4\text{-}H)(\mu_3\text{-}Cu)_4(Se_2P(OR)_2)_6]^+$ (see Scheme 3). Thus two T energy minima can be tentatively postulated for a $[Cu_4Ag_4(H)(Se_2PH_2)_6]^+$ species. On the other hand, one may anticipate that the clusters containing a second- or third-row encapsulated ion, which are of T_h symmetry in the homometallic series, should correspond in the bimetallic $[Cu_4Ag_4(X)(Se_2PH_2)_6]^q$ series to a single energy mimimum of T symmetry in which X is octacoordinated. The question of the number of T minima is less straightforward for the X = F and X = O cases which present a small and moderate tetrahedral distortion in the homometallic species, respectively. To provide a conclusive answer to this question, we have looked for the number of minima of T symmetry in the $[Cu_4Ag_4(X)(Se_2PH_2)_6]^q$ (X = □, H, F, Cl, Br, O, S and Se) (see Table 5).

Scheme 3. Two Possible Arrangements of T Symmetry for a $[Cu_4Ag_4(\mu_4\text{-}H)(Se_2P(OR)_2)_6]^+$ Species

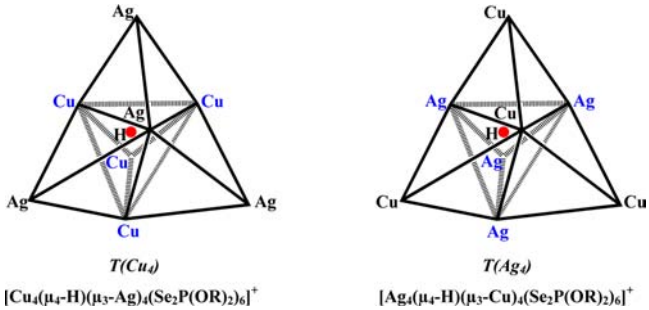

A unique minimum was found for the empty cluster $[Cu_4Ag_4(Se_2PH_2)_6]^{2+}$ (X = □), in which surprisingly the Ag_4 tetrahedron is of smaller size than the Cu_4 one, although the Ag–Ag separations remain large (4.70 Å). In the case of X = H, two tetracapped tetrahedral isomers are found in which the hydride is clearly tetracoordinated. The most stable (by 0.50 eV) corresponds to the hydride being bonded to four silver atoms. In the case of X = F and O, a unique minimum is found in which X is tetracoordinated to the four Ag and Cu atoms, respectively. These preferences will be discussed later. When X = Cl, Br, S, and Se, the encapsulated anion is found to be octacoordinated. Comparing the M–X distances of these mixed metal compounds to their homologues in the homometallic series suggests that in the former Ag–X bonding is stronger than Cu–X for X = Cl, S, and Se. This difference is particularly substantial in the case of chlorine which indicates a clear tendency to tetracoordination to silver (see Table 5).

dx.doi.org/10.1021/ic400959a | Inorg. Chem. 2013, 52, 7752–7765

Table 5. Relevant Computed Data Corresponding to the Optimized Geometries of $[Cu_4Ag_4(X)(Se_2PH_2)_6]^q$ (X = □, H, F, Cl, Br, O, S, Se)[a]

q	$[Cu_4Ag_4(X)(Se_2PH_2)_6]^q$	symm.	Cu_1-Ag_1(Å), Cu_1-Cu_2(Å), Ag_1-Ag_2 (Å)	Cu−X (Å), Ag−X (Å)
+2	X = □		3.45	3.09
		T	5.04	2.88
			4.70	
+1	X = H		2.90	1.79
		T(*Cu*$_4$) (Δ*E* = 0.50)[b]	2.91	2.95
			4.81	
			2.97	2.98
		T(*Ag*$_4$) (Δ*E* = 0.00)[b]	4.87	1.97
			3.21	
	X = F		3.22	3.06
		T(*Ag*$_4$)	4.98	2.46
			4.02	
	X = Cl		3.38	2.99
		T	4.88	2.85
			4.65	
	X = Br		3.41	2.88
		T	4.71	3.02
			4.93	
0	X = O		2.93	2.02
		T(*Cu*$_4$)	3.31	2.90
			4.73	
	X = S		3.05	2.36
		T	3.84	2.87
			4.69	
	X = Se		3.13	2.51
		T	4.09	2.89
			4.72	

[a] *T*(*Cu*$_4$) and *T*(*Ag*$_4$) refer to the two possibilities of tetracoordination of X, respectively, as sketched for X = H in Scheme 3. [b] Relative energies between different isomers.

5. EXPERIMENTAL STRUCTURES OF FLUORINE- AND OXYGEN-CENTERED CLUSTERS

5.1. Fluorine-Centered Species. Several X-ray structures of octanuclear dithio- or diseleno-phosphate Cu(I) or Ag(I) clusters encapsulating Cl, Br, S or Se are known.[4,5] They all exhibit clear octacoordination of the encapsulated anion, with a geometry which can be idealized in T_h symmetry, in agreement with our computed results. On the other hand, the clusters encapsulating a hydride have been shown experimentally to afford a strong tetrahedral distortion,[7,8] still in full agreement with our calculations (see above). The case of fluorine is less straightforward, since the theoretically predicted tetrahedral distortion is rather small, although significant (DI ∼ 20%), and associated with a very small energy stabilization of a few hundredth of eVs. This raises the question of the significance of this value at our level of theory. Even assuming it is significant, it is of the order of magnitude of other distortion energies caused by steric or crystal packing forces and consequently, the tetrahedral distortion might be difficult to evidence in X-ray molecular structures. This is why we have carried out the synthesis of the hexafluorophosphate salts of three new fluorine-containing cationic clusters, namely, $[Cu_8(F)(S_2P(OR)_2)_6](PF_6)$ [R = ^{i}Pr (**1**), Et (**2**)] and $[Ag_8(F)(S_2P(O^nPr)_2)_6](PF_6)$ (**3**) and compared their X-ray structures with those of the related fluorine-containing octahedral Cu(I) and Ag(I) clusters which are already known. Their synthesis and characterizations are reported in the Supporting Information.

Clusters **1**−**3** have been characterized by the single-crystal X-ray diffraction technique. The general structure feature consists of a discrete cationic cluster in which eight copper (or silver) ions are linked by six face-capping (μ_2, μ_2) dithiophosphate ligands and a central F^- ion with a noncoordinating PF_6^- anion. The eight metal atoms are arranged at the corner of a somewhat distorted cube.[1c] The monocationic octanuclear copper cluster **1** crystallizes in the monoclinic space group *C*2/*c* with the encapsulated F(1) atom located on the center of inversion. The symmetry point group of cluster **1** is C_i (Figure 2a) with four crystallographically independent Cu−F distances, that is, Cu(1)−F(1) = 2.6272(7) Å, Cu(2)−F(1) = 2.5930(7) Å, Cu(3)−F(1) = 2.6526(8) Å, and Cu(4)−F(1) = 2.6405(7) Å. Thus, the fluoride-centered Cu_8 core geometry approaches that of a perfect cube, with a slight compression along the Cu(2)−F(1)−Cu(2A) axis as illustrated by solid Cu−F bonds in Figure 2a (see also Table 6). The core of the molecule is very similar to the reported structure of $[Cu_8(F)\{Se_2P(O^iPr)_2\}_6]^+$.[7a] The Cu−S distances [2.2415(13)−2.2674(13) Å] are comparable to those in $[Cu_8(Cl)(S_2P(O^iPr)_2)_6]^+$ [2.2642(22)−2.2915(21) Å].[5f] Compound **2** crystallizes in the trigonal space group $R\bar{3}c$. Four copper atoms are found in the asymmetric unit where the 3-fold rotational axis passes through Cu(2), F(1), and Cu(4) (Figure 2b). In this compound, the F(1) atom does not locate exactly in the center of the cluster which is of C_3 symmetry, but close to tetrahedral symmetry as exemplified by the existence of four shorter Cu−F bonds [1 × Cu(2)−F1 = 2.563(6) and 3 × Cu(3)−F(1) = 2.493(2)] and four longer Cu−F bonds ([3 × Cu(1)−F(1) = 2.635(2) and 1 × Cu(4)−F(1) = 2.627(6)]. The core geometry of compound **2** can be well described as a fluoride-centered tetracapped tetrahedron

dx.doi.org/10.1021/ic400959a | Inorg. Chem. 2013, 52, 7752−7765

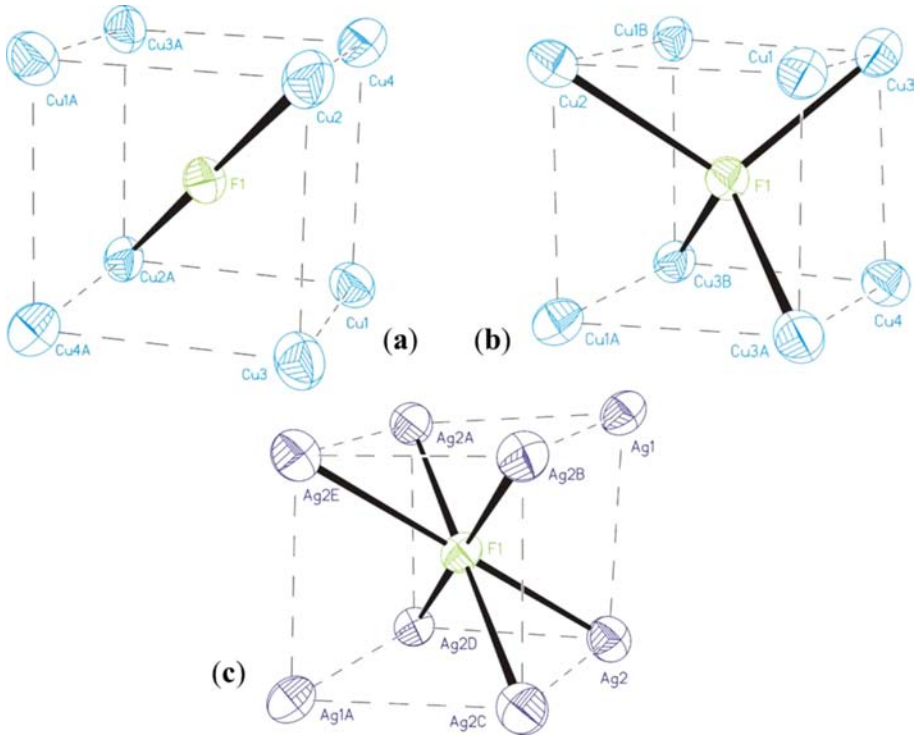

Figure 2. Perspective views (30% displacement ellipsoid) of (a) the $[Cu_8(F)]$ core in **1**; (b) the $[Cu_8(F)]$ core in **2**; (c) the $[Ag_8(F)]$ core in **3**. Selected bond lengths (Å) for **1**: Cu(1)−Cu(3), 3.0009(10); Cu(1)−Cu(2A), 3.0501(10); Cu(2)−Cu(4), 3.0016(10); Cu(2)−Cu(3), 3.0299(10); Cu(2)−Cu(1A), 3.0500(10). Selected bond lengths (Å) for **2**: Cu(1)−Cu(2), 3.0402(12); Cu(1)−Cu(3), 3.0114(13); Cu(1)−Cu(3A), 2.8843(13); Cu(2)−Cu(1A), 3.0403(12). Cu(2)−Cu(1B), 3.0402(12). Selected bond lengths (Å) for **3**: Ag(1)−Ag(2), 3.2374(6); Ag(2)−Ag(2C), 3.1084(6).

Table 6. Metric Data of the Known Clusters of the Type $[M_8(F)(E_2P(OR)_2)_6]^+$ (M = Cu, Ag; E = S, Se)

compound	ref.	M−M[a] range and average (Å)	M−E[b] range and average (Å)	DI (%)[d]
$[Cu_8(F)(S_2P(O^iPr)_2)_6]^+$	*c*	3.001−3.050 (3.035)	2.257−2.268 (2.261)	
$[Cu_8(F)(S_2P(OEt)_2)_6]^+$	*c*	2.884−3.041 (2.971)	2.240−2.281 (2.265)	10
$[Cu_8(F)(Se_2P(^iPr)_2)_6]^+$	3	2.970−3.086 (3.040)	2.354−2.377 (2.367)	
$[Cu_8(F)(Se_2P(OEt)_2)_6]^+$	3	2.911−3.130 (3.010)	2.334−2.392 (2.363)	8
$[Ag_8(F)(S_2P(O^nPr)_2)_6]^+$	*c*	3.108−3.238 (3.173)	2.496−2.528 (2.512)	
$[Ag_8(F)(S_2P(OEt)_2)_6]^+$	4	3.036−3.259 (3.129)	2.408−2.586 (2.510)	29

[a]M = Cu, Ag. [b]E = S, Se. [c]This work. [d]Distortion index measuring the degree of tetrahedral distortion away from the ideal T_h cubic structure (if any), as defined in the text.

with Cu(2), Cu(3), and its symmetry-generated counter parts as the capping atoms. The average Cu−Cu distance [2.971(2) Å] is slightly shorter than those observed in **1**, [3.035(2) Å]. Compound **3** crystallizes in the trigonal space group $R\bar{3}$. Two silver atoms are located in the asymmetric unit with the C_3 rotational axis passing through Ag(1), F(1), and Ag(1A) atoms, leading to the S_6 point group symmetry for the cluster (Figure 2c). With six shorter Cu−F(1) distances of 2.6566(3) Å and two longer Cu−F(1) distances of 3.0044(7) Å along the C_3 axis, the Ag_8 cube affords a bicapped octahedral distortion as sketched in the middle of Scheme 1. The Ag−Ag distances in the range 3.1084(6)−3.2374(6) Å and Ag−S distances in the range of 2.4958(13)−2.5283(13) are comparable to those in $[Ag_8(F)(S_2P(OEt)_2)_6](PF_6)$ [3.036(12)−3.259(12) Å].[8b]

Thus, among the three investigated species, only one exhibits a tetrahedral distortion. Looking at the other known fluorine-encapsulating clusters (Table 6), it appears that two of them, namely, $[Cu_8(F)(Se_2P(OEt)_2)_6]^+$ and $[Ag_8(F)(Se_2P(OEt)_2)_6]^+$, are also tetrahedrally distorted. The average T_h to T distortion index of the former (8%) compares well with that of its diseleno analogue **2** (10%), whereas that of the latter is larger (29%). Thus, the predicted tetrahedral distortion is experimentally proven to exist, although only half of the structurally characterized compounds exibit it in the solid state. Interestingly, these three compounds are dichalcogeno diethyl phosphate derivatives, that is, are those bearing the less bulky ligands. These results confirm that, although weak, the predicted forces which are driving the tetrahedral distortion in these fluorine derivatives are real and in some cases can overrun the packing and/or steric distortion forces. This provides confidence for other results on compounds which have not been yet synthesized.

5.2. Oxygen-Centered $Cu_4Ag_4(O)(Se_2P(OEt)_2)_6$ Cluster. Although there are plenty of oxide-centered $Cu(II)_4$ structures of the type, $Cu_4(\mu_4\text{-}O)(\mu\text{-}X)_4L_4$ (X = halide, L = two-electron donor ligand),[26] it should be noted that **4** is to our knowledge the first example of an encapsulated oxide inside a Cu(I) and/or Ag(I) cluster. Despite being of limited quality arising from severe disorders of the metal framework, its X-ray structure is in a surprisingly good agreement with the optimized geometry of the $Cu_4Ag_4(O)(Se_2PH_2)_6$ model. It crystallizes in the monoclinic space group $R\bar{3}$ and exhibits two overlapping Cu_8 and Ag_8 cubes, each being 50% occupancy, with an oxygen

dx.doi.org/10.1021/ic400959a | Inorg. Chem. 2013, 52, 7752−7765

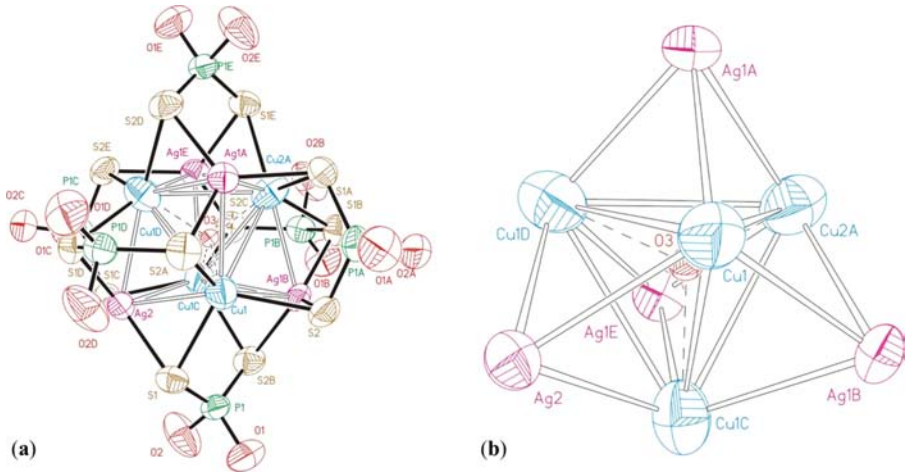

Figure 3. Perspective views (30% displacement ellipsoid) of (a) $Cu_4Ag_4(O)(S_2P(OEt)_2)_6$ (**4**) (ethyl groups omitted for clarity), (b) the $Cu_4(O)Ag_4$ core of **4**. Selected bond lengths (Å): Cu−Cu, 3.415(6)−3.363(6), Cu−Ag, 2.920(4)−2.935(4), Cu−O3, 2.003(8)−2.100(5), Ag−O3, 2.841−2.886, Ag−Ag, 4.641−4.678 Å.

atom in their common center. They can be deconvoluted into two oxygen-centered tetracapped tetrahedral $Cu_4(\mu_4\text{-}O)(\mu_3\text{-}Ag)_4$ cores of the *T(Cu₄)* type sketched on the left side of Scheme 3. The resulting X-ray structure of **4** is shown in Figure 3. It is of C_3 symmetry, but close to perfect tetrahedral arrangement. The averaged Cu−O and Ag−O distances, respectively 2.07 Å and 2.85 Å, are close to the corresponding optimized values of $Cu_4Ag_4(O)(Se_2PH_2)_6$ which are 2.02 Å and 2.90 Å, respectively. The averaged Cu−Cu, Ag−Ag, and Cu−Ag distances (3.39 Å, 4.66 Å and 2.92 Å, respectively) are also in good agreement with the optimized ones (3.31 Å, 4.73 Å, and 2.93 Å, respectively). Thus, taken as a whole, the experimental and optimized structures confirm the tendency for tetrahedral distortion in the oxygen-centered octanuclear species.[26]

6. BONDING ANALYSIS

The covalent component of the bonding between an encapsulated 8-electron main-group anion X^{q-2} and its $[M_8(E_2PH_2)_6]^{2+}$ (M = Cu, Ag; E = S, Se) hosting cage in the ideal T_h cubic symmetry can be understood from the qualitative MO diagrams of Figures 4 and 5. In the empty cage, discarding the weak M(I)−M(I) (d^{10}-d^{10}) interaction, each metal atom lies in an almost perfect trigonal planar local coordination, allowing a stable 16-electron configuration. In such a situation, there is a low-lying nonbonding unoccupied valence p_z orbital on each metal center, perpendicular to its coordination plane and therefore pointing toward the center of the cube. At the considered metal−metal distances, the eight diffuse p_z orbitals somehow overlap and give rise in the T_h symmetry to four antibonding (of t_g and a_u symmetry) and four bonding (of t_u and a_g symmetry) unoccupied combinations (middle of Figure 4). The latter ones constitute a nice set of low-lying accepting orbitals having the proper symmetry to interact with the four occupied valence s and p orbitals of the encapsulated X^{q-2} anion (Figure 5). In the case of an encapsulated hydride, only the lowest one (the a_g combination) is involved. Distorting the T_h cubic cage into a tetracapped tetrahedron of *T* symmetry results in a stabilization of the fully symmetrical accepting orbital (now of "a" symmetry) and an increase of its localization on the central tetrahedron. Thus, the tetrahedral distortion enhances the accepting ability of the "a"

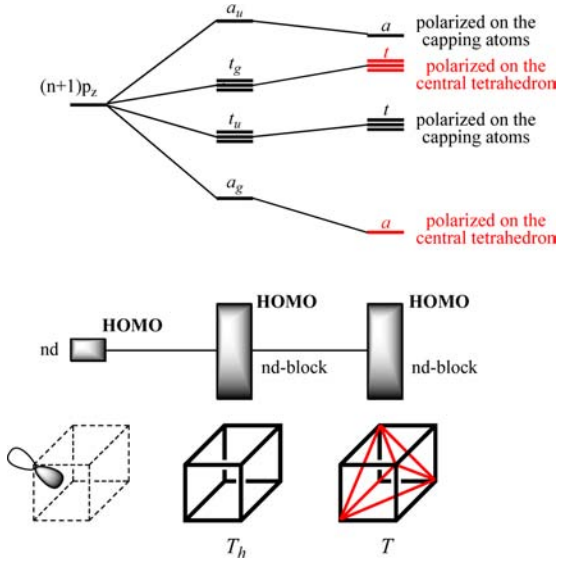

Figure 4. Metal-based frontier MO diagram of an octanuclear cage $[M_8(E_2PH_2)_6]^{2+}$ (M = Cu, Ag; E = S, Se). Middle: Cubic shape; right: Tetracapped tetrahedral shape.

orbital. On the other hand, this distortion tends to somehow destabilize the triply degenerate accepting orbitals (now of "t" symmetry) and to localize them preferentially on the four capping metals (right side of Figure 4). Thus, the tetrahedral distortion of the empty cage reduces the accepting ability of its t orbitals and consequently does not favor sp^3 hybridization of the encapsulated main group anion.

We start the quantitative bonding analysis by considering the most relevant data computed for the $[Cu_8(X)(S_2PH_2)_6]^q$ series which are reported in Table 7. The dissociation energy (DE) is computed as the difference between the sum of the energies of X^{q-2} and of $[M_8(\square)(E_2PH_2)_6]^{2+}$ in its equilibrium geometry and the energy of $[M_8(X)(E_2PH_2)_6]^q$ in its equilibrium geometry. The computed DE has no physical meaning per se, since computing the energy of an isolated anion has no physical meaning in molecular chemistry (even discarding the potential problems of computing anion energies). However, it constitutes a good qualitative tool for comparing the bonding within series of anions of the same charge, that is, H^-, F^-, Cl^-, Br^- or O^{2-},

dx.doi.org/10.1021/ic400959a | *Inorg. Chem.* 2013, 52, 7752−7765

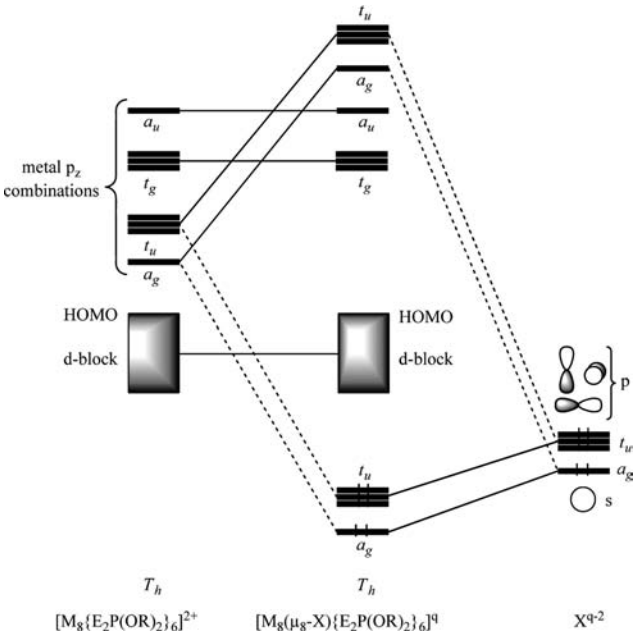

Figure 5. Interaction MO diagram between an encapsulated 8-electron main-group anion and its cubic $[M_8(E_2PH_2)_6]^{2+}$ (M = Cu, Ag; E = S, Se) hosting cage of T_h symmetry.

S^{2-}, Se^{2-}. The bonding energy (BE) is defined as the difference between the sum of the energies of X^{q-2} and the $[M_8(\square)(E_2PH_2)_6]^{2+}$ fragment in the frozen geometry it adopts in $[M_8(X)(E_2PH_2)_6]^{2+}$ and the energy of $[M_8(X)(E_2PH_2)_6]^q$ in its equilibrium geometry. For similar reasons as for DEs, BEs can only be used for comparing series of clusters containing anions of same formal charge. The difference between BE and DE (ΔE_{Dist}) is simply the amount of energy required for distorting the relaxed $[M_8(\square)(E_2PH_2)_6]^{2+}$ cage into the geometry it adopts in $[M_8(X)(E_2PH_2)_6]^q$. Thus DE = BE − ΔE_{Dist}. One can see that ΔE_{Dist} is minimum and small (∼ 0.15 eV) for Cl^- and Br^-. This was expected since these anions require only a small cage distortion. Whereas ΔE_{Dist} is large in the case of X = H (∼ 1. eV), the T_h to T distortion requires little energy. A similar conclusion can be traced for X = F and O. Looking now at the DEs in the monoanionic series, one can see that it varies in the order $H^- > F^- > Cl^- > Br^-$, despite that H^- requires much larger ΔE_{Dist} than Cl^- or Br^-, for example. This means that DE is largely dominated by BE. A similar conclusion can be traced for the dianionic series ($O^{2-} > S^{2-} > Se^{2-}$), whereas ΔE_{Dist} is almost constant within the series. In the case of N^{3-}, and C^{4-}, BE and ΔE_{Dist} could not be computed for the S_6 and C_3 minima because of convergence problems. For these particular cases, one may anticipate compensations between larger BEs and ΔE_{Dist} values for the corresponding energy minima.

BE can be approximated as the sum of a covalent component and an ionic component. Not surprisingly, the weaker covalent interaction between the encapsulated anion and the dicationic cage corresponds to X = F, as exemplified by the lower computed anion-to-cation charge transfers and Cu-X Wiberg indices (Table 7). The rather long Cu−F distance in the optimized T_h geometry (Table 2) is also consistent with a dominant ionic bonding. A similar conclusion can be traced for Cl^- and Br^-. In contrast, the larger charge transfer and Wiberg indices computed for H^- indicate a substantially larger Cu-X covalent character, which increases upon tetrahedral distortion

Table 7. Relevant Bonding Parameters Computed for $[Cu_8(X)(S_2PH_2)_6]^q$ (X = H, F, Cl, Br, I, q = +1; X = O, S, Se, q = 0; X = N, P, q = −1; X = C, q = −2)[a]

q	$[Cu_8(X)(S_2PH_2)_6]^q$	symm.	BE (eV)	DE (eV)	ΔE_{Dist} (eV)	Cu-X Wiberg indices[b]	NAO charge and population analysis of X
+1	X = H	T	11.70	10.65	1.05	4×0.103 4×0.006	−0.64 ($1s^{1.64}$)
		T_h	11.12	10.23	0.89	8×0.045	−0.68 ($1s^{1.68}$)
	X= F	T	9.42	9.16	0.26	4×0.035 4×0.016	−0.86 ($2s^{1.97}$ $2p^{5.88}$)
		T_h	9.31	9.15	0.16	8×0.025	−0.86 ($2s^{1.98}2p^{5.88}$)
	X = Cl	T_h	7.77	7.65	0.12	8×0.036	−0.83 ($3s^{1.95}$ $3p^{5.86}$)
	X = Br	T_h	7.20	7.02	0.18	8×0.040	−0.82 ($4s^{1.95}$ $4p^{5.84}$)
0	X = O	T	26.79	25.93	0.86	4×0.083 4×0.023	−1.70 ($2s^{1.92}$ $2p^{5.77}$)
		T_h	26.49	25.75	0.74	8×0.054	−1.68 ($2s^{1.94}$ $2p^{5.73}$)
	X = S	T_h	21.84	21.06	0.78	8×0.079	−1.60 ($3s^{1.87}$ $3p^{5.68}$)
	X = Se	T_h	20.06	19.31	0.75	8×0.081	−1.59 ($4s^{1.88}$ $4p^{5.66}$)
−1	X = N	S_6	*c*	47.18	*c*	6×0.206 2×0.032	−2.15 ($2s^{1.74}$ $2p^{5.38}$)
		C_3	*c*	45.98	*c*	3×0.175 3×0.088 1×0.064 1×0.037	−2.33 ($2s^{1.83}2p^{5.47}$)
		T_h	47.35	45.69	1.66	8×0.090	−2.42 ($2s^{1.85}2p^{5.54}$)
	X = P	T_h	38.05	36.33	1.71	8×0.131	−2.24 ($3s^{1.76}$ $3p^{5.41}$)
−2	X = C	S_6	*c*	64.81	*c*	6×0.277 2×0.027	−2.74 ($2s^{1.59}$ $2p^{5.11}$)
		T_h	64.73	61.76	2.97	8×0.142	−3.01 ($2s^{1.85}2p^{5.54}$)

[a]BE, bonding energy; DE, dissociation energy; ΔE_{Dist}, cage distortion energy (see text for definitions). [b]Expressed in the NAO basis. [c]Could not be calculated because of convergence problems.

dx.doi.org/10.1021/ic400959a | Inorg. Chem. 2013, 52, 7752−7765

(compare averages of the 8 Cu-X Wiberg indices). Thus, the strong tetrahedral distortion afforded by the hydride-centered species is a size effect substantially driven by covalent interactions. The case of O^{2-} is less straightforward. Although larger than F^- in size, it affords a significantly larger tetrahedral distortion, whereas, according to the NAO population analysis this distortion is not associated with an increase of covalency. Indeed, when going from T_h to T, the anion-to-cation charge transfer slightly decreases (because of a weaker participation of the 2p(O) orbitals not fully compensated by a stronger 2s(O) participation) and the average Cu-X Wiberg index decreases in constrast to the X = F and H cases. These results suggest that, although the covalent character of the Cu−O bonding is significant, it is its ionic component which is driving the tetrahedral distortion. Despite its larger size, the encapsulated oxygen bears a much larger negative charge than its fluorine homologue, inducing in turn stronger electrostatic interactions with the cationic cage, leading to a larger tetrahedral distortion. With any encapsulated elements larger than oxygen, the tetrahedral distortion is not favored and the T_h cubic architecture of the cage is maintained, except for nitrogen and carbon which prefer lying in an octahedral environment.

Similar results as those of Table 7 were found for the three other series, that is, M = Cu, E = Se and M = Ag, E = S, Se (see Supporting Information, Tables S4, S5 and S6). Interestingly, larger DEs were found in the case of M = Ag for X = F (weak covalent interaction) whereas in the case of X = H and O larger DEs were found for M = Cu (significant covalent interaction). These results are consistent with those reported in Table 5 which show a preference for F to bond to Ag whereas H and O prefer to bond to Cu.

7. DYNAMICS OF THE HYDRIDE-CONTAINING SPECIES

Previous NMR investigations on the compounds $[Ag_8(H)(Se_2P(OR)_2)_6](PF_6)$ (R = ^{i}Pr, Et) indicate that the encapsulated proton is coupled to eight magnetically equivalent ^{109}Ag nuclei at room temperature, whereas both the X-ray and DFT-computed structures consist of a μ_4-hydride encapsulated in an $Ag_4(\mu_3\text{-}Ag)_4$ tetracapped tetrahedron.[8a] These results indicate that the four inner and the four capping silver atoms are exchanging their positions at a faster rate than the typical time scale of the NMR measurement. No doubt that the same phenomenon occurs also for the copper-hydride homologues. The simplest interconversion mechanism between the small 1−3−6−8 tetrahedron and large 2−4−5−7 tetrahedron sketched on the left side of Scheme 1 is to go through a regular cube, that is, a structure of T_h symmetry for the $[M_8(H)(E_2PH_2)_6]^+$ species under investigation. However, the number of imaginary vibrational frequencies calculated for the T_h structures (Table 2 and Supporting Information, Tables S1−S3) indicates that they are not intermediates nor transition states. Moreover, their computed relative energies with respect to the corresponding T minima are too large to be consistent with the expected fast reaction rate. This is why we have looked for a low-symmetry pathway interconverting the two degenerate T minima in the case of the $[Cu_8(H)(Se_2PH_2)_6]^+$ model. In our search for possible low-symmetry intermediates, two secondary minima of C_{2h} and C_{2v} symmetry, respectively, were found. Their skeletons are sketched in Figure 6. As in the T minimum, their hydride is tetracoordinated, but this time in an approximate square-planar mode rather than in a tetrahedral one. In the 4-fold degenerate

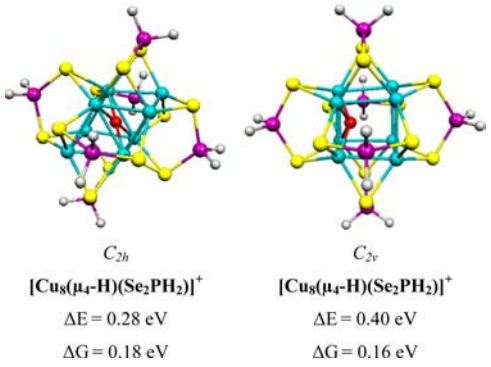

Figure 6. Two secondary energy minima of $[Cu_8(H)(Se_2PH_2)_6]^+$. ΔE and ΔG are their relative energies and Gibbs free energies with respect to the global minimum shown in Figure 1.

C_{2h} minimum, the hydride sits in the middle of a rectangular face shared by two fused triangular prisms. Surprisingly this near square-planar μ_4-H coordination mode is geometrically similar to that of the three interstitial μ_4-H existing in a nanospheric copper polyhydride, $[Cu_{20}(H)_{11}(S_2P(O^iPr)_2)_9]$, recently reported by us.[27] In the 6-fold degenerate C_{2v} minimum it lies close to the middle of one of the faces of a distorted cube. Their relative energies with respect to the T minimum are 0.28 and 0.40 eV, respectively, that is, they are lower than that of the corresponding T_h structure (0.54 eV). This makes the C_{2h} minimum a good candidate as possible intermediate in the process of interconversion between the two T minima.

Unfortunately, the search for transition states involving any of the two energy minima $[Cu_8(H)(Se_2PH_2)_6]^+$ turned out to be unsuccessful. However, the flat potential energy surface of this entity and the significant difference between ΔE and ΔG in Figure 6, suggests it could be that thermal fluctuations would play a significant role in the hydride dynamics that would prevent a proper characterization of the intermediates. Thus, to take these fluctuations into account, we have undertaken molecular dynamics simulations of the $[Cu_8(H)(S_2PH_2)_6]^+$ species. To discriminate between the various structures visited along the simulations, a proper set of order parameters is to be defined. We have used two of them that are the coordination number of the hydride with the 1−3−6−8 Cu atoms and noted CV_1 (corresponding initially to the small Cu tetrahedron in Scheme 1) and the coordination number of the hydride with the 2−4−5−7 Cu atoms noted CV_2 (corresponding initially to the large Cu tetrahedron in Scheme 1). These two parameters allow to monitor both the coordination scheme of the hydride and the interconversion of the two tetrahedra. Indeed, the initial T minimum corresponds to the {0 ; 4} configuration and a full interconversion of the tetrahedra would lead to the {4 ; 0} configuration. The T_h structure corresponds to the {0 ; 0} configuration.

Figure 7a represents the density plot obtained at 300 K for a 16.5 ps long simulation. As can be seen, the species is not trapped in the initial configuration {0 ; 4} but freely shuttles between the {4 ; 0}, {3 ; 0}, {2 ; 0}, {3 ; 1}, {2 ; 1}, and {1 ; 1} configurations. Consequently, the energy barriers between these local metastable states are rather low, that is, of the order of k_BT. This is in full agreement with the liquid state ^{109}Ag and ^{1}H NMR measurements in solution and the observation of only one hydride signal as our simulation suggests that, at ambient temperature, $[Cu_8(H)(S_2PH_2)_6]^+$ visits a whole set of

dx.doi.org/10.1021/ic400959a | Inorg. Chem. 2013, 52, 7752−7765

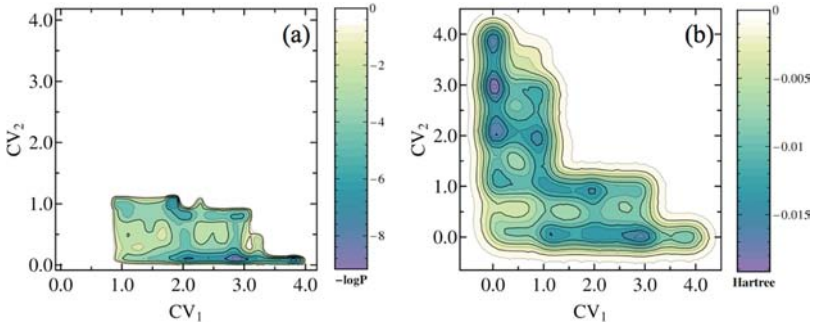

Figure 7. (a) Density plot of the configurations explored during a nonbiased 300 K MD simulation of the $[Cu_8(H)(S_2PH_2)_6]^+$ species. The configurations are discriminated in terms of $\{CV_1 ; CV_2\}$ couples. (b) FES of the $[Cu_8(H)(S_2PH_2)_6]^+$ species obtained from a MetaD simulation at 300 K using CV_1 and CV_2 as CVs.

configurations that could be part of the interconversion mechanism between the two tetrahedra. The NMR observation requires that this interconversion occurs on a time scale lower than the millisecond (the characteristic time of the NMR measurement) which seems to be the case seeing our short simulation. However, during our accessible time scale, we have not observed a full interconversion because of the usual sampling limitations of ab initio MD. To overcome this problem, we have then conducted MD simulations in combination with the metadynamics approach. The ability of this method to study activated process has already been demonstrated for various chemical problems[28] but, to the best of our knowledge, this is the first application to metal cluster chemistry. In MetaD, the MD simulation is biased using a history dependent potential that allows the systems to escape from local minima. When fully converged, the history dependent potential converges toward the opposite of the free energy surface (FES). The construction of the history dependent potential decreases the dimensionality of the problem as it is constructed based on a limited number of user-defined order parameters, the collective variables. The CVs are characteristic of the evolution of the system of interest.

We have performed MetaD simulations at 300 K of the $[Cu_8(H)(S_2PH_2)_6]^+$ species using as CVs, CV_1 and CV_2. The use of these two CVs greatly reduces the overall dimensionality of the hydride dynamics problem. However, by symmetry, CV_1 and CV_2 are sufficient to describe the dominant transitions that can occur. Figure 7b displays the resulting two-dimensional FES which is symmetric with respect to the diagonal of the plot because of the chosen set of CVs. This FES suggests that the cluster never goes through the T_h structure ($\{0 ; 0\}$ configuration). Although not properly converged, the difference in free-energy between the $\{0 ; 4\}$ and $\{0 ; 0\}$ basins are of the order of ∼0.4 eV, in accordance with the results of Table 1. In contrast, the interconversion process appears to be composed of a succession of Cu−H bonds breaking and forming that leads to a wealth of intermediate structures populating the $\{4 ; 0\}$, $\{3 ; 0\}$, $\{2 ; 0\}$, $\{1 ; 0\}$, $\{3; 1\}$, $\{2 ; 1\}$ and $\{1 ; 1\}$ basins. Supporting Information, Figure S2 gathers some representative configurations belonging to these basins. As can be seen in Supporting Information, Figure S2, the previously characterized intermediate of C_{2v} symmetry (see Figure 6b) is also found in the $\{2 ; 2\}$ region during our MetaD simulation but at a really high free-energy. Unfortunately, although the underlying mechanism we have depicted is correct, it is not possible to extract accurate free-energy differences because of the difficulty to properly converge an ab initio MetaD simulation for such a complex system. Moreover, it is expected that the inclusion of nuclear quantum effects in our simulations would greatly smoothen the FES, making the interconversion process easier, if not almost barrierless.

Considering this unconcerted character, it is not surprising that a global transition state is difficult to characterize by transition-state-search formalisms. However, all the states belonging to the diagonal of Figure 7b would prove to be key structures in this process. Indeed, below this line, the hydride is mainly bonded to the initially small tetrahedron and above to the initially large tetrahedron. On the diagonal, the hydride is equally bonded to both tetrahedra. As a consequence, we can consider that the interconversion has partially occurred when the system crosses this line. It is worth pointing out that the two intermediates of Figure 6 are both $\{2 ; 2\}$ configurations located on this line.

8. CONCLUDING REMARKS

The softness of the cubic M_8L_6 cage (M = Cu(I), Ag(I); L = dichalcogeno ligand) and the 16-electron configuration of the metal centers confer it the ability to encapsulate various kinds of atomic anions, adapting easily its shape for maximizing the host−guest bonding interaction. The interplay between size, covalent and ionic bonding favors either the cubic, tetrahedral, or bicapped octahedral structure of the metal framework. Whereas the large third- and fourth-row main group anions maintain the cubic shape, a distortion toward a tetracapped tetrahedral arrangement of the metals occurs in the case of hydride, fluoride, and oxide, as proven both by X-ray structures and DFT calculations. The distortion is strong in the case of hydride, weak (and not always observable) in the case of fluoride, and intermediate in the case of oxide. DFT calculations predict a bicapped octahedral architecture in the case of nitride and carbide. Although it was isolated serendipitously, the characterization of the first oxide-containing cluster of this type, $Cu_4Ag_4(O)(Se_2P(OEt)_2)_6$, indicates that such species are stable and suggests similar arguments for nitride-centered species. The design of new synthetic approaches remains however to be found. Finally, for the first time, we have been able to confirm, using ab initio MetaD simulations, the dynamical behavior of the hydride-centered species which was experimentally suggested. Moreover, we have been able to characterize the interconversion mechanism between two tetracapped tetrahedral configurations. In contrast with what could have been expected, this process occurs in a rather unconcerted mechanism, through a succession of Cu−H bonds breaking and forming involving a

dx.doi.org/10.1021/ic400959a | Inorg. Chem. 2013, 52, 7752−7765

rather large number intermediate structures, and with very low activation energy. A refinement of our simulations could incorporate nuclear quantum effects that would certainly lead to smoother energy barriers and thus would prove important to accurately characterize the temperature dependence of this dynamical behavior.

■ ASSOCIATED CONTENT

Ⓢ Supporting Information

Synthesis and characterization procedures for compounds **1**−**4**. Complementary data computed for clusters of the type $[M_8(X)(E_2PH_2)_6]^q$ (M = Cu, Ag; E = S, Se; X = □ (vacancy), H, F, Cl, Br, O, S, Se, N, P, C). Cartesian coordinates and total energy of all the computed structures. This material is available free of charge via the Internet at http://pubs.acs.org.

■ AUTHOR INFORMATION

Corresponding Author

*E-mail: saillard@univ-rennes1.fr.

Notes

The authors declare no competing financial interest.

■ ACKNOWLEDGMENTS

Financial support from the National Science Council of Taiwan (NSC 100-2113-M-259-003) is gratefully acknowledged. Professor M. Parinello is acknowledged for his kind advice. The Swiss National Supercomputing Center and High Performance Computing Group of ETH Zurich are thanked for computational resources. J.Y.S. thanks the Institut universitaire de France for support.

■ REFERENCES

(1) (a) Lobana, T. S.; Wang, J.-C.; Liu, C. W. *Coord. Chem. Rev.* **2007**, *251*, 91−110. (b) Liu, C. W.; Woollins, J. D. In *Selenium and Tellurium Chemistry*; Woolins, J. D., Laitinen, R. S., Eds.; Springer-Verlag: Berlin, Germany, 2011; Chapter 13, pp 303−320. (c) Haiduc, I. In *Handbook of Chalcogen Chemistry: New Perspectives in Sulfur, Selenium and Tellurium*; Devillanova, F. A., Ed.; RSC: Cambridge, U.K., 2006.

(2) Garland, M. T.; Halet, J.-F.; Saillard, J.-Y. *Inorg. Chem.* **2001**, *40*, 3342−3350.

(3) (a) McCandish, L. E.; Bissel, E. C.; Coucouvanis, D.; Fackler, J. P., Jr.; Knox, K. *J. Am. Chem. Soc.* **1968**, *90*, 7357. (b) Hollander, F. J.; Coucouvanis, D. *J. Am. Chem. Soc.* **1974**, *96*, 5647. (c) Hollander, F. J.; Coucouvanis, D. *J. Am. Chem. Soc.* **1977**, *99*, 6268. (d) Dietrich, H. *Acta Crystallogr.* **1978**, *A32*, S26. (e) Dietrich, H.; Storck, W.; Manecke, G. *Makromol. Chem.* **1981**, *182*, 2371. (f) Hanhui, Z.; Xiufen, Y. *Jiegou Huaxue (J. Struct. Chem.)* **1989**, *8*, 132.

(4) (a) Birker, P. J. M. W. L.; Freeman, H. C. *J. Am. Chem. Soc.* **1977**, *99*, 6890. (b) Birker, P. J. M. W. L. *Inorg. Chem.* **1979**, *18*, 3502. (c) Schugar, H. J.; Ou, C.-C.; Thich, J. A.; Potenza, J. A.; Felthouse, T. R.; Haddad, M. S.; Hendrickson, D. N.; Furey, W., Jr.; Lalancette, R. A. *Inorg. Chem.* **1980**, *19*, 543. (d) Wu, D.; Huang, J. Q.; Lin, Y.; Huang, J. L. *Sci. Sin. Ser. B. (Engl. Ed.)* **1988**, *31*, 800. (e) Huang, Z. X.; Lu, S. F.; Huang, J. Q.; Wu, D. M.; Huang, J. L. *Jiegou Huaxue (J. Struct. Chem.)* **1991**, *10*, 213. (f) Liu, C. W.; Stubbs, T.; Staples, R. J.; Fackler, J. P., Jr. *J. Am. Chem. Soc.* **1995**, *117*, 9778.

(5) (a) Liu, C. W.; Shang, L.-J.; Wang, J.-C.; Keng, T.-C. *Chem. Commun.* **1999**, 995−996. (b) Liu, C. W.; Hung, C.-M.; Haia, H.-C.; Liaw, B.-J.; Liou, L.-S.; Tsai, Y.-F.; Wang, J.-C. *Chem. Commun.* **2003**, 976−977. (c) Liu, C. W.; Hung, C.-M.; Santra, B. K.; Chen, H.-C.; Hsueh, H.-H.; Wang, J.-C. *Inorg. Chem.* **2003**, *42*, 3216−3220. (d) Liu, C. W.; Hung, C.-M.; Santra, B. K.; Wang, J.-C.; Kao, H.-M.; Lin, Z. *Inorg. Chem.* **2003**, *42*, 8551−8556. (e) Liu, C. W.; Haia, H.-C.; Hung, C.-M.; Santra, B. K.; Liaw, B.-J.; Lin, Z.; Wang, J.-C. *Inorg. Chem.* **2004**, *43*, 4464−4470. (f) Liu, C. W.; Irwin, M. D.; Mohamed, A. A.; Fackler, J. P., Jr. *Inorg. Chim. Acta* **2004**, *357*, 3950−3956.

(6) (a) Liu, C. W.; Feng, C.-S.; Fu, R.-J.; Chang, H.-W.; Saillard, J.-Y.; Kahlal, S.; Wang, J.-C.; Chang, I.-Jy. *Inorg. Chem.* **2010**, *49*, 4934−4941. (b) Liu, C. W.; Chang, H.-W.; Liao, P.-K.; Fang, C.-S.; Saillard, J.-Y.; Kahlal, S. *J. Cluster Sci.* **2011**, *22*, 381−396. (c) Li, Y.-J.; Latouche, C.; Kahlal, S.; Liao, J.-H.; Dhayal, R. S.; Saillard, J.-Y.; Liu, C. W. *Inorg. Chem.* **2012**, *51*, 7439−7441.

(7) (a) Liu, C. W.; Sarkar, B.; Huang, Y.-J.; Liao, P.-K.; Wang, J.-C.; Saillard, J.-Y.; Kahlal, S. *J. Am. Chem. Soc.* **2009**, *131*, 11222−11233. (b) Liao, P.-K.; Sarkar, B.; Chang, H.-W.; Wang, J.-C.; Liu, C.-W. *Inorg. Chem.* **2009**, *48*, 4089−4097.

(8) (a) Liu, C. W.; Chang, H.-W.; Sarkar, B.; Saillard, J.-Y.; Kahlal, S.; Wu, Y.-Y. *Inorg. Chem.* **2010**, *49*, 468−475. (b) Liu, C. W.; Chang, H.-W.; Fang, C.-S.; Sarkar, B.; Wang, J.-C. *Chem. Commun.* **2010**, *46*, 4571−4573.

(9) (a) Liao, P.-K.; Liu, K.-G.; Fang, C.-S.; Liu, C. W.; Fackler, J. P., Jr.; Wu, Y.-Y. *Inorg. Chem.* **2011**, *50*, 8410−8417. (b) Liao, P.-K.; Fang, C.-S.; Edwards, A. J.; Kahlal, S.; Saillard, J.-Y.; Liu, C. W. *Inorg. Chem.* **2012**, *51*, 6577−6591. (c) Liao, P.-K.; Shi, D.-R.; Liao, J.-H.; Liu, C. W.; Artem'ev, A. V.; Kuimov, V. A.; Gusarova, N. K.; Trofimov, B. A. *Eur. J. Inorg. Chem.* **2012**, *30*, 4921−4929.

(10) (a) Liu, C. W.; Liao, P.-K.; Fang, C.-S.; Saillard, J.-Y.; Kahlal, S.; Wang, J.-C. *Chem. Commun.* **2011**, *47*, 5831−5833. (b) Liu, C. W.; Lin, Y.-R.; Fang, C.-S.; Latouche, C.; Kahlal, S.; Saillard, J.-Y. *Inorg. Chem.* **2013**, *52*, 2070−2077.

(11) Frisch, M. J.; Trucks, G. W.; Schlegel, H. B.; Scuseria, G. E.; Robb, M. A.; Cheeseman, J. R.; Montgomery, J. A. Jr.; Vreven, T.; Kudin, K. N.; Burant, J. C.; Millam, J. M.; Iyengar, S. S.; Tomasi, J.; Barone, V.; Mennucci, B.; Cossi, M.; Scalmani, G.; Rega, N.; Petersson, G. A.; Nakatsuji, H.; Hada, M.; Ehara, M.; Toyota, K.; Fukuda, R.; Hasegawa, J.; Ishida, M.; Nakajima, T.; Honda, Y.; Kitao, O.; Nakai, H.; Klene, M.; Li, X.; Knox, J. E.; Hratchian, H. P.; Cross, J. B.; Adamo, C.; Jaramillo, J.; Gomperts, R.; Stratmann, R. E.; Yazyev, O.; Austin, A. J.; Cammi, R.; Pomelli, C.; Ochterski, J. W.; Ayala, P. Y.; Morokuma, K.; Voth, G. A.; Salvador, P.; Dannenberg, J. J.; Zakrzewski, V. G.; Dapprich, S.; Daniels, A. D.; Strain, M. C.; Farkas, O.; Malick, D. K.; Rabuck, A. D.; Raghavachari, K.; Foresman, J. B.; Ortiz, J. V.; Cui, Q.; Baboul, A. G.; Clifford, S.; Cioslowski, J.; Stefanov, B. B.; Liu, G.; Liashenko, A.; Piskorz, P.; Komaromi, I.; Martin, R. L.; Fox, D. J.; Keith, T.; Al-Laham, M. A.; Peng, C. Y.; Nanayakkara, A.; Challacombe, M.; Gill, P. M. W.; Johnson, B.; Chen, W.; Wong, M. W.; Gonzalez, C.; Pople, J. A. *Gaussian 03*, revision B. 04; Gaussian, Inc.: Pittsburgh, PA, 2003.

(12) (a) Becke, A. D. *Phys. Rev. A* **1988**, *38*, 3098−30100. (b) Perdew, J. P. *Phys. Rev. B* **1986**, *33*, 8822−8824.

(13) Weigend, F.; Ahlrichs, R. *Phys. Chem. Chem. Phys.* **2005**, *7*, 3297−3305.

(14) Glendening, E. D.; Badenhoop, J. K.; Reed, A. E.; Carpenter, J. E.; Bohmann, J. A.; Morales, C. M.; Weinhold, F. *NBO 5.0*; Theoretical Chemistry Institute, University of Wisconsin: Madison, WI, 2001; http://www.chem.wisc.edu/nbo5.

(15) Car, R.; Parrinello, M. *Phys. Rev. Lett.* **1985**, *55*, 2471−2474.

(16) Troullier, N.; Martins, J. L. *Phys. Rev. B* **1991**, *43*, 1993.

(17) Ceriotti, M.; Bussi, G.; Parrinello, M. *J. Chem. Theor. Comput.* **2010**, *6*, 1170−1180.

(18) Bonomi, M.; Branduardi, D.; Bussi, G.; Camilloni, C.; Provasi, D.; Raiteri, P.; Donadio, D.; Marinelli, F.; Pietrucci, F.; Broglia, R. A.; Parrinello, M. *Comput. Phys. Commun.* **2009**, *180*, 1961−1972.

(19) Barducci, A.; Bussi, G.; Parrinello, M. *Phys. Rev. Lett.* **2008**, *100*, 020603.

(20) *SAINT V4.043: Software for the CCDC Detector System*; Bruker Analytical X-ray System: Madison, WI, 1995.

(21) Sheldrick, G. M. *SADABS*; University of Göttingen: Göttingen, Germany, 1996.

(22) Sheldrick, G. M. *Acta Crystallogr.* **2008**, *A64*, 112−122.

(23) *SHELXL 5.10 (PC version): Program Library for Structure Solution and molecular Graphics*; Bruker Analytical X-ray System: Madison, WI, 1998.

(24) Alvarez, S. *Dalton Trans.* **2005**, 2209−2233.
(25) We thank one of the reviewers for warning us about the difference between the stellated tetrahedron (DI = 100%), a concave polyhedron, and the triakis tetrahedron (DI = − 61%), a convex polyhedron. Both polyhedra can be viewed as distorted cubes. See Casanova, D.; Llunell, M.; Alemany, P.; Alvarez, S. *Chem.—Eur. J.* **2005**, *11*, 1479−1494.
(26) Melnik, M.; Koman, M.; Ondrejovi, G. *Coord. Chem. Rev.* **2011**, *255*, 1581−1586.
(27) Dhayal, R. S.; Liao, J.-H.; Lin, Y.-R.; Liao, P.-K.; Kahlal, S.; Saillard, J.-Y.; Liu, C. W. *J. Am. Chem. Soc.* **2013**, *135*, 4704−4707.
(28) (a) Laio, A.; Gervasio, F. L. *Rep. Prog. Phys.* **2008**, *71*, 126601. (b) Barducci, A.; Bonomi, M.; Parrinello, M. *WIREs Comput. Mol. Sci.* **2011**, *1*, 826−843.

dx.doi.org/10.1021/ic400959a | *Inorg. Chem.* 2013, 52, 7752−7765